Mandana Jalali*, Andreas Prokscha, Yijun Yan, Tobias Kubiczek, Jan Taro Svejda, Sascha Preu, Jan Balzer, Thomas Kaiser, and Daniel Erni

Non-invasive glucose sensing via the fingernail bed using THz radiation

https://doi.org/10.1515/cdbme-2023-1127

Abstract: The possibility of establishing a novel technique for reliably accessing glycemic information in a non-invasive, easy to implement method at THz frequencies via the fingernail bed is investigated. The nail bed's major content is blood at its various glucose levels and is also partially protected from environmental conditions by the nail plate, making it a desirable platform for non-invasive glucose sensing. The study is based on a 2D computational electromagnetics (EM) model of the layered fingernail in COMSOL Multiphysics, where the required dielectric function (i.e. permittivity and conductivity) of the fingernail plate is measured using THz-Time-Domain-Spectroscopy (THz-TDS), and the glucose-dependend dielectric functions of the fingernail bed are taken from available experimental data in the literature. From this data a material model using a multipole Cole-Cole model is established for both, the nail plate and the nail bed, where the glucose content in the latter is varied from 3.0-19.0 mmol/l. A numerical analysis of the THz reflectometry at the fingernail in the frequency range of 0.1-2.0 THz revealed that the reflectance spectra are sensitive to the glucose content in the nail bed proving that accurate glucose sensing via the fingernail bed may become feasible around 0.2-0.4 THz.

Keywords: Diabetes, Glucose sensing, Fingernail bed, Cole-Cole model, THz radiation, THz-TDS.

***Corresponding author: Mandana Jalali,** General and Theoretical Electrical Engineering (ATE), Faculty of Engineering, University of Duisburg-Essen, and CENIDE – Center for Nanointegration Duisburg- Essen, D-47048 Duisburg, Germany, e-mail: mandana.jalali@uni-due.de

Andreas Prokscha and Thomas Kaiser, Institute of Digital Signal Processing, Faculty of Engineering, University of Duisburg-Essen, D-47048 Duisburg, Germany.

Yijun Yan, Jan Taro Svejda, and Daniel Erni, General and Theoretical Electrical Engineering (ATE), Faculty of Engineering, University of Duisburg-Essen, and CENIDE – Center for Nanointegration Duisburg- Essen, D-47048 Duisburg, Germany.

Tobias Kubiczek and Jan Balzer, Chair of Communication Systems, Faculty of Engineering, University of Duisburg-Essen, D-47048 Duisburg, Germany.

Sascha Preu, Terahertz Devices and Systems, Institute of Microwave Engineering and Photonics, Department of Electrical Engineering and Information Technology, Technical University of Darmstadt, D-64283 Darmstadt, Germany.

1 Introduction

Diabetes mellitus has become a major public health problem with global epidemic dimensions where one in ten adults worldwide suffers from diabetes. Correspondingly, finding a non-invasive, easy-to-use method to reliably access glycemic information from the blood's glucose content (providing reliable warnings for hyperglycemia and hypoglycemia) can significantly improve the life quality of diabetes patients. The first truly non-invasive device as an alternative to the amperometric analysis of extracted blood samples has been developed by Pendragon in 2004 using impedance respective dielectric spectroscopy in the 1-200 MHz range at the skin surface [1]. The strong conductivity variations in the stratum corneum and epidermis under varying environmental and physiological conditions (e.g. moisture, sweating) rendered the overall accuracy to become inferior compared to the conventional invasive approach [2]. A comprehensive analysis of a dielectric spectroscopy setting using sophisticated fringing-field electrodes in conjunction with a highly accurate multi-scale, multi-layer skin model aimed rather in support of this fundamental limitation [3]. Nevertheless, using (multi-GHz) transmission measurements, e.g. through the earlobe or the skin fold between index finger and thumb may become promising as they allow for a de-embedding of the uncertainties in the top skin layer [4]. Alternatively, wearable optical glucose sensors at the skin surface (using visible and IR wavelengths) are currently investigated as an extension to photo-plethysmography [5], whereas non-invasive multi-spectral optical glucose monitoring with form factors reaching from desktop devices to wrist watch sized sensors are still under development [6]. Referring to the mentioned fundamental limitations we therefore propose a compact THz reflectometry at the fingernail bed as this tissue surface has a less complex morphology, is precisely defined, well perfused and even protected by the (transparent) nail plate.

2 Material properties

Corresponding material properties for both, the nail plate and the nail bed are required within a frequency range of 0.1-2.0 THz. For the nail plate, experimental THz-TDS in the range of 0.5-1.5 THz has been carried out, where the fingernail plate (here one author's

thumbnail) with the size of 7 mm × 12 mm and an average thickness of 0.503 mm (cf. Figure 1 inset), was grown for about 4 month and cut to obtain the required sample. The flat area in the fingernail centre is used for the measurements as the edges are curved and hence not appropriate for material characterization measurements. The commercial fiber-coupled THz spectrometer TERA K15 from Menlo Systems is used to generate and detect THz radiation, where the system has a single shot dynamic range of 65 dB and a single shot bandwidth of about 4 THz. The nail plate is mounted in the focused part of the THz transmission setup (cf. Figure 1), and is repeatedly remounted eight times not only to include different positions along the flat surface, but also to support a statistical analysis which improves the accuracy. A pinhole is used to align the nail plate with a 3D printed holder to the intended focus position. For each position, 200 THz-TDS traces are recorded and averaged ($\underline{E}_{\text{sample}}(\omega)$), together with a reference ($\underline{E}_{\text{ref}}(\omega)$) trace without the fingernail plate. The complex permittivity $\underline{\varepsilon}_r = \varepsilon_r'(\omega) - j\varepsilon_r''(\omega)$ is then determined through calculating the transfer function $\underline{T}(\omega) = \underline{E}_{\text{sample}}(\omega)/\underline{E}_{\text{ref}}(\omega)$ for each of the recorded THz-TDS traces [7]. By extracting the phase $\varphi(\omega)$ from $\underline{T}(\omega)$, the refractive index $n(\omega)$ can be calculated (cf. Eq. (1)).

$$n(\omega) = 1 + \frac{\varphi(\omega)c_0}{\omega d} \tag{1}$$

Where c_0 is the speed of light in vacuum and d is the sample thickness. Accordingly, $\varepsilon_r'(\omega)$ and $\varepsilon_r''(\omega)$ can be calculated using the following equations.

$$\varepsilon_r' = (1 + n(\omega))^2 - \frac{c_0^2}{\omega^2 d^2} \ln\left(\frac{(n(\omega)+1)^2}{4n(\omega)}|\underline{T}(\omega)|\right) \tag{2}$$

$$\varepsilon_r'' = \frac{c_0}{\omega^2} n(\omega) \ln\left(\frac{(n(\omega)+1)^2}{4n(\omega)}|\underline{T}(\omega)|\right) \tag{3}$$

The complex permittivity is then calculated by averaging over all 8 recorded THz-TDS traces, and are illustrated in the Figure 2.

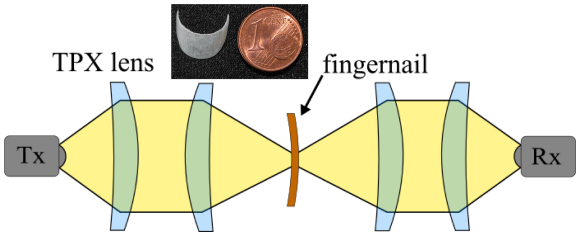

Figure. 1: Schematic of THz-TDS transmission measurement setup for determining the dielectric function of the nail plate. TPX lenses are used to focus the terahertz radiation generated by the introduced THz-TDS system. The fingernail is placed in the focus spot. The thumbnail is shown next to a euro-cent coin.

The material properties of the perfused nail bed are taken from the specific literature [8, 9], where the dielectric functions within the frequency range of 0.3-0.5 THz are given for various glucose contents namely, 3.0 mmol/l, 3.8 mmol/l, 6.2 mmol/l, 9.2 mmol/l, 11.0 mmol/l, 14.9 mmol/l, 18.0 mmol/l, and 19.0 mmol/l. As neither of the available data cover the whole frequency range of interest, based on these data sets two 4-pole Cole-Cole models [10] have been developed; one for the nail plate and a glucose-dependent one for the nail bed where each is given by the following the relation

$$\underline{\varepsilon}_r = \varepsilon_\infty + \sum_{i=1}^{4} \frac{\Delta\varepsilon_i}{1 + (j\omega\tau_i)^{(1-\alpha_i)}} + \frac{\sigma_s}{j\omega\varepsilon_0} \tag{4}.$$

Here ε_∞ is the relative high-frequencies permittivity, σ_s is the static conductivity, τ_i stands for the i-th relaxation time, $\Delta\varepsilon_i$ labels the i-th permittivity increment, and α_i is the i-th broadening parameter (according to the distribution of relaxation times). Each Cole-Cole model is fitted to its corresponding data set, where the underlying 14 coefficients are retrieved from an evolutionary algorithm-based optimization procedure, which minimizes the least-square error between the model and the experimental data.

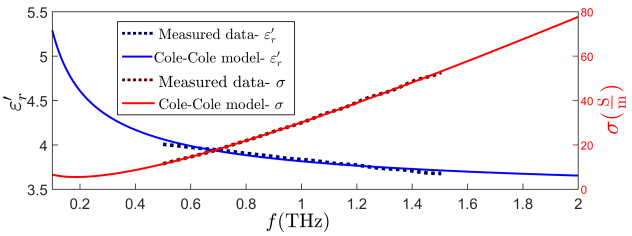

Figure. 2: Nail plate – The retrieved dielectric function from the Cole-Cole model (solid lines) and the underlying measured data, namely the permittivity and conductivity (dotted lines).

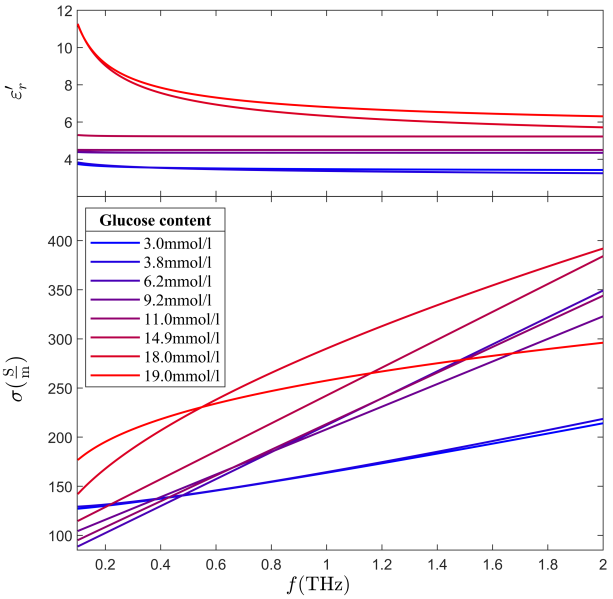

Figure. 3: Nail bed – The retrieved dielectric function showing the Cole-Cole model of permittivity (top), and conductivity (bottom), where the color codes relate to the corresponding glucose levels in the nail bed. A dependence of conductivity on aqueous glucose is shown in [11].

Table 1: The coefficients of the fitted 4-pole Cole-Cole model of the nail plate according to Eq. 4.

$\Delta\varepsilon_1$	$\Delta\varepsilon_2$	$\Delta\varepsilon_3$	$\Delta\varepsilon_4$	$\tau_1(\mathrm{ps})$	$\tau_2(\mathrm{ps})$	$\tau_3(\mathrm{ns})$	$\tau_4(\mu\mathrm{s})$
117.4	44.6	7.1	2.3	726.4	895.4	641.6	637.0
α_1	α_2	α_3	α_4	ε_∞	$\sigma_s(\mathrm{S/m})$		
0.4	0.4	0.7	2.0	1.0	2.2		

For the nail plate the frequency dependent permittivity and conductivity are illustrated in Figure 2 for both, the measured data and the fitted Cole-Cole model, where the coefficients are summarized in the Table 1.

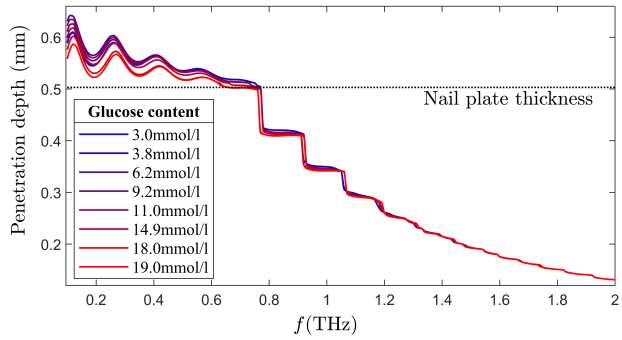

Figure. 4: The spectral response of the simulated 1/e penetration depth of the electric field for all mentioned glucose levels. The dotted black line indicates the nail plate thickness.

The glucose dependent permittivities and conductivities of the nail bed are depicted in the Figure 3. Interestingly, the real part of the permittivities show a rather linear increase with increasing glucose content, whereas the conductivities show a rather irregular but potentially unique behavior, which may be further exploited in glucose sensing.

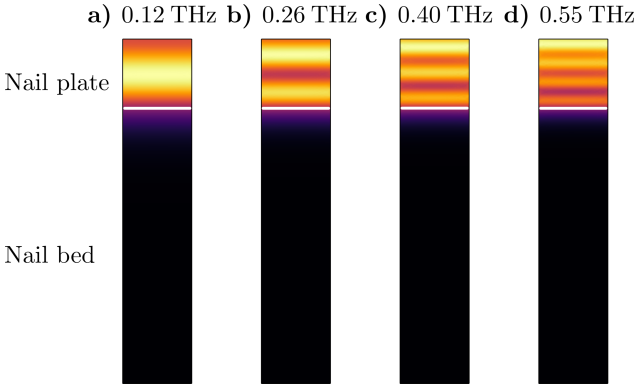

Figure. 5: Simulated absolute value of the electric field distributions (a.u.) within the layers of the finger nail at (a) 0.12 THz, (b) 0.26 THz, (c) 0.40 THz, and (d) 0.55 THz, showing weak Fabry-Pérot fringes in the nail plate. The white line indicates the nail plate/bed interface.

3 Penetration depths

In order to investigate the interaction of the fingernail with an impinging THz radiation and accordingly, to study the feasibility of glucose sensing via fingernail reflectometry, a corresponding 2D layered computational electromagnetics model is set up in the FEM-based simulation platform COMSOL Multiphysics using the developed material models. The thickness of the nail plate is set to 0.503 mm according to the measured nail plate, and the nail bed is considered to be 2 mm thick. The fingernail structure is then illuminated with a plane wave covering the frequency range of 0.1-2.0 THz. To determine specific spectral windows where the electric field in the nail bed is potentially enhanced and therefore more suitable for glucose sensing, the 1/e penetration depth of the electric field into the nail structure was analyzed. The resulting spectral dependencies of the penetration depth with respect to all mentioned glucose contents are depicted in the Figure 4.

In the range of 0.1-0.6 THz, the field attenuation is small and, accordingly, the penetration depth becomes resonantly enhanced yielding values larger than the thickness of the nail plate. For example, as shown for a glucose content of 3.0 mmol/l, the spectral response exhibits peaks at 0.12 THz, 0.26 THz, 0.40 THz, and 0.55 THz (which undergo a slight blue shift with increasing glucose content). This is due to weak Fabry-Pérot fringes that are formed in the nail plate with electric field distributions as depicted in Figure 5.

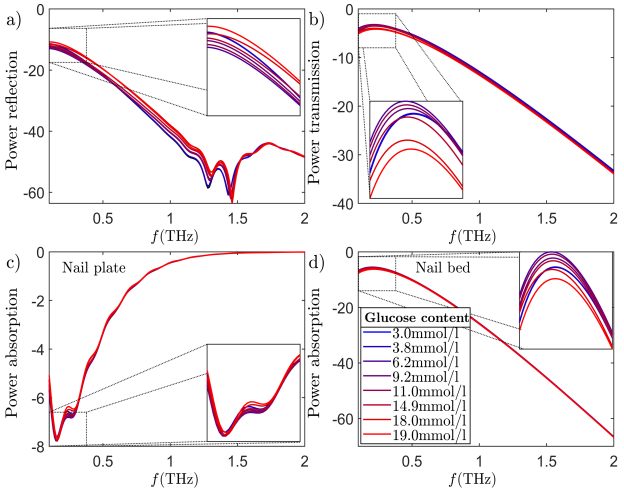

Figure. 6: Simulated spectral responses of the corresponding power flow in the finger nail for various glucose contents, where the insets zoom into the most relevant frequency range of 0.1-0.4 THz according to the sensitivity of power absorption and reflection against glucose levels. (a) Power reflection coefficient at the nail plate, (b) the coefficient of the power transmission into the nail bed, (c) the relative absorbed power integrated over the nail plate, and (d) the relative absorbed power integrated over the nail bed. A preliminary estimate yields a reflectance sensitivity of around 0.2 dB/(mmol/l).

4 Reflection and absorption

In order to establish potential detection criteria for a reliable glucose sensing via the fingernail bed, the power reflection coefficient from the finger nail, the coefficient of the power transmission into the nail bed, as well as the relative absorbed power within each layer are studied. The results are presented in Figure 6 and show distinct changes in the spectral responses of the power reflection, power transmission, as well as in the integrated relative power absorption with respect to given variations of the glucose level. Accordingly, glucose sensing via the nail bed reflectometry seems effective especially in the range of 0.1-0.4 THz, where the mentioned changes in the reflected and absorbed power are more prominent. It is worth noting that the observed changes of these power spectra due to glucose variations display irregular frequency-dependent alterations with potentially non-trivial dependencies to the proper glucose levels. At a single spectral position these alterations are, though, not well pronounced, implying that a proper glucose analysis has to rely on additional frequency samples aiming at intensive multi-spectral (or broadband) data processing in conjunction machine-learning-based inverse problem solving.

A 3D model of the fingernail, based on the nail anatomy (cf. Figure 7a)) is created and simulated for the case of 3.0 mmol/l glucose content in the nail bed. The absolute values of the electric field distribution within the nail layers at 0.4 THz for the cases of 3D nail model as well as the 2D layered model are presented in the Figure 7, where it is shown that in the nail center the field distributions are quite similar. However, apart from the nail center the observed Fabry-Pérot fringes are accordingly distorted due to the presence of the edge (cf. inset of Figure 7b).

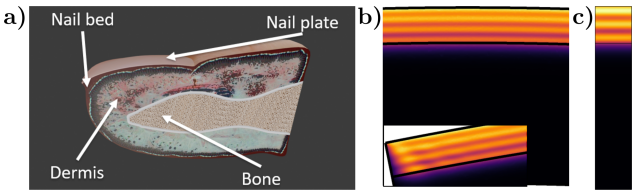

Figure. 7: a) Nail anatomy showing the inner structures of the nail. Simulated absolute value of the electric field distributions within the layers of the finger nail at 0.4 THz, showing weak Fabry-Pérot fringes in the nail plate for the b) 3D nail model, incorporating nail layers curvature, where the inset depicts the electric field distribution at the edge of the nail, and c) 2D layered nail model.

5 Conclusion and outlook

In this numerical study based on a two-layer model of the fingernail with realistic tissue properties, we provided a first proof-of-concept, that glucose sensing via nail bed reflectometry may be feasible especially in the frequency range of 0.1-0.4 THz. The proper choice of the suitable frequency window is thus mainly driven by the discussed sensitivity against glucose level variations but also by the bandwidth of a potential multi-spectral approach to reliably solve the mentioned inverse problem (in real time). Within this spectral window, higher operation frequencies are usually preferred to support an ultra-compact implementation with form factors corresponding to easy-to-carry PoC devices. A comprehensive 3D numerical proof-of-concept is currently underway based on photorealistic fingernail models (including natural variations of nail plates) in conjunction with (conformal) THz antenna structures that mimic the transceiver interface.

Acknowledgments

The research presented in this paper is partially funded by the Deutsche Forschungsgemeinschaft (DFG) Project-ID 287022738 TRR 196 MARIE for Projects C02, M01, M03, M05, S04, and S05, in part by the Ministry of Culture and Science of the State of North Rhine-Westphalia (MKW NRW) through Project terahertz.NRW, and in part by the German Federal Ministry of Education and Research (BMBF) in the course of the 6GEM research hub under grant number 16KISK038.

References

[1] Caduff A, Hirt E, Feldman Y, Ali Z, Heinemann L. First human experiments with a novel non-invasive, non-optical continuous glucose monitoring system, Biosens Bioelectron 2003; 19(3):209-217.

[2] Weinzimer SA. PENDRA: The Once and Future Noninvasive Continuous Glucose Monitoring Device? Diabetes Technol Ther 2004; 6(4):442-444.

[3] Huclova S, Baumann D, Talary MS, Froehlich J. Sensitivity and specificity analysis of fringing-field dielectric spectroscopy applied to a multi-layer system modelling the human skin, 2011; Phys Med Biol 56(24):7777-7793.

[4] Pikov V, Siegel PH. US Patent No US11229383B2, 2022.

[5] Rachim VP, Chung WY. Wearable-band type visible-near infrared optical biosensor for non-invasive T blood glucose monitoring, Sens Actuators B Chem 2019; 286:173-180.

[6] DiaMonTech AG, Berlin: https://www.diamontech.de.

[7] Jepsen PU, Cooke DG, Koch M. Terahertz spectroscopy and imaging–Modern techniques and applications. Laser Photonics Rev 2011; 5(1):124-166.

[8] Guseva VA, Demchenko PS, Litvinov EA, Cherkassova OP, Meglinski IV, Khodzitsky MK. Study of glucose concentration influence on blood optical properties in THz frequency range. Nanosyst: Phys Chem Math 2018; 9(3):389–400.

[9] Guseva VA, Gusev SI, Demchenko PS, Sedykh EA, Khodzitsky MK. Optical properties of human nails in THz frequency range. J Biomed Photonics Eng 2016; 2(4):40306.

[10] Gabriel S, Lau RW, Gabriel C. The dielectric properties of biological tissues: III. Parametric models for the dielectric spectrum of tissues. Phys Med Biol 1996; 41(11):227.

[11] Song C, Fan WH, Ding L, Chen X, Chen ZY, Wang K. Tera-hertz and infrared characteristic absorption spectra of aqueous glucose and fructose solutions, Sci Rep 2018; 8:8964.